Effect of a laser prepulse on a narrow-cone ejection of MeV electrons from a gas jet irradiated by an ultrashort laser pulse

Tomonao Hosokai,[1,*] Kenichi Kinoshita,[2] Alexei Zhidkov,[2] Kei Nakamura,[1] Takahiro Watanabe,[1] Toru Ueda,[1] Hideyuki Kotaki,[3] Masaki Kando,[3] Kazuhisa Nakajima,[3,4] and Mitsuru Uesaka[1]

[1]*Nuclear Engineering Research Laboratory, Graduate School of Engineering, University of Tokyo, 22-2 Shirane-shirakata, Tokai, Naka, Ibaraki, 319-1188, Japan*

[2]*Department of Accelerator Physics and Engineering, National Institute of Radiological Sciences, 4-9-1, Anagawa, Inage, Chiba, 263-8555 Japan*

[3]*Advanced Photon Research Center, Kansai Research Establishment, Japan Atomic Energy Research Institute, 8-1 Umemi-dai, Kizu, Soraku, Kyoto, 619-0215 Japan*

[4]*High Energy Accelerator Research Organization (KEK), Tsukuba, Ibaraki 305-0801, Japan*

(Received 1 October 2002; published 25 March 2003)

Spatial and energy distributions of energetic electrons produced by an ultrashort, intense laser pulse with a short focal length optical system (Ti:sapphire, 12 TW, 50 fs, $\lambda = 790$ nm, $f/3.5$) in a He gas jet are measured. They are shown to depend strongly on the contrast ratio and shape of the laser prepulse. The wave breaking of the plasma waves at the front of the shock wave formed by a proper laser prepulse is found to make a narrow-cone (0.1π mm mrad) electron injection. These electrons are further accelerated by the plasma wake field generated by the laser pulse up to tens of MeV forming a Maxwell-like energy distribution. In the case of nonmonotonic prepulse, hydrodynamic instability at the shock front leads to a broader, spotted spatial distribution. The numerical analysis based on a two-dimensional (2D) hydrodynamic (for the laser prepulse) and 2D particle-in-cell (PIC) simulation justifies the mechanism of electron acceleration. The PIC calculation predicts that electrons with energy from 10 to 40 MeV form a bunch with a pulse duration of about 40 fs.

DOI: 10.1103/PhysRevE.67.036407 PACS number(s): 52.38.Kd, 41.75.Jv, 52.38.−r, 52.38.Hb

I. INTRODUCTION

Particle acceleration via laser-plasma interactions has been studied intensively for many years. Among a number of concepts of the particle acceleration by laser fields, the laser wake-field acceleration (LWFA) in underdense plasma [1] provides one of the most promising approaches to high performance compact electron accelerators. Until recently, a wake field of the order of 100 GeV/m in a plasma has been observed in LWFA experiments [2–5]. Furthermore, since it has a relatively small length of acceleration [5], the LWFA, particularly, allows the production of an ultrashort electron bunch ($\sim$10 fs) for probe analysis of matter [6]. However, electron injection into the wake field is a crucial part for LWFA. Since the typical length of the wake field of the plasma wave is the order of $2\pi\omega_{pl}/c \sim 10$–$100$ μm, the length of the injected electron bunch must be 2–20 μm. Usually for LWFA, the injection of a high quality electron beam from a conventional rf (radio-frequency)-driven linac accelerator is assumed [2]. In other schemes, two or several laser pulses are employed for the injection [3,4]. However, such schemes require highly precise synchronization between the wake field and the injection. One of the simplest ways to put energetic electrons into the wake field for their further acceleration is the wave breaking of plasma waves produced by a single intense laser pulse [5]. Though such injection gives a broad Maxwell-like energy distribution of accelerated electrons, a transverse geometrical emittance of electron bunch can be much better than that from the conventional linac.

The basic properties of the wave breaking are well known [7]. If the intensity of the laser pulse is not very high (see Ref. [8]), the wave breaking appears when the plasma wave amplitude exceeds the threshold $E_B \sim [2(\omega/\omega_{pl} - 1)]^{1/2} mc\omega_{pl}/e$, where ω and ω_{pl} are the laser and plasma frequency. This occurs in a plasma with a rather steep density profile, $\lambda_{pl} dN/dx \sim 1$, $\lambda_{pl} = 2\pi\omega_{pl}/c$, where λ_{pl} is the wavelength of the plasma wave [9]. However in a gas jet, the density gradient is much smaller; since usually $N/(dN/dx) \sim 200/500$ μm, the injection originating from the wave breaking of the plasma waves hardly happens if only the main laser pulse is coming. Practically, a laser prepulse with approximately a few nanoseconds duration precedes the main laser pulse [10]. The usual contrast ratio varies from $1{:}10^5$ to $1{:}10^7$ for fundamental laser frequency. If the Rayleigh length L_R is short enough, the prepulse can form a cavity with a shock wave in front of the laser propagation. In contrast to the plasma channel produced by a long Rayleigh length laser prepulse [11–14], the length of the cavity is determined by this small L_R, because the energy is deposited in the plasma mostly near the focus point $x = 0$ as $W(x) \sim 1/[1 + (x/L_R)^2]$, where $W(x)$ is the energy of a laser prepulse deposited at x, and x is a coordinate in the laser propagation direction. Since the laser prepulse has low intensity, the electron temperature T_e can be estimated via the collisional absorption mechanism [16], $dT_e/dt = \Delta\varepsilon\, \nu_{ei}(1\text{ eV})/T_e^{3/2}$, where $\Delta\varepsilon = 2\pi e^2 I/m\omega^2$ is the energy acquired by an electron in a collision, I is the laser intensity, and ν_{ei} is the frequency of electron-ion collisions. For inten-

*Electronic address: hosokai@tokai.t.u-tokyo.ac.jp

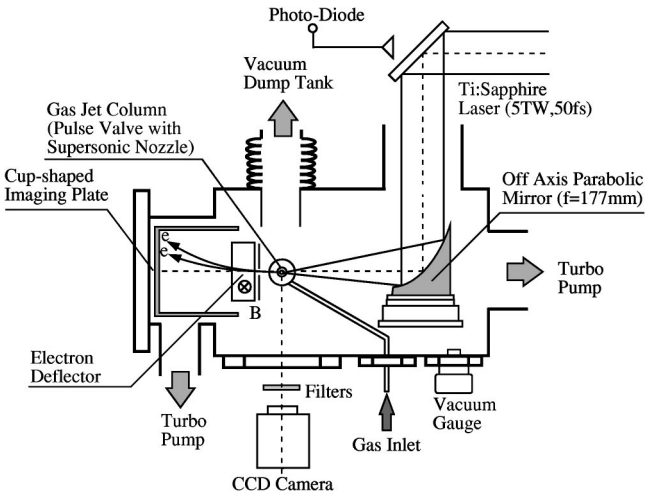

FIG. 1. Experimental setup.

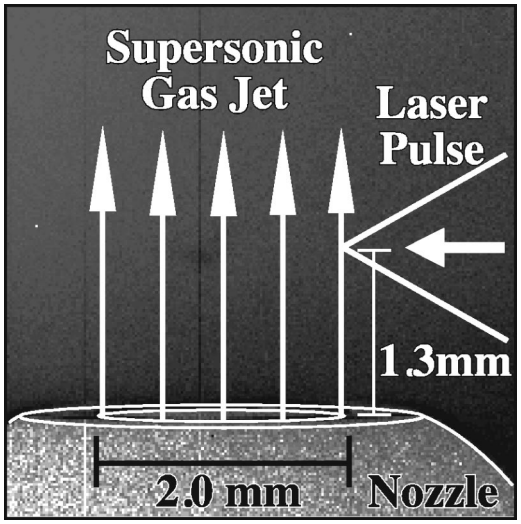

FIG. 2. CCD image of the interaction region. Supersonic gas jet and laser focus position is illustrated in the inset.

sity $I=10^{13}$ W/cm^2, final ion density $N_i=3\times10^{18}$ cm^{-3} (in the cavity), and pulse duration $\tau=2$ ns, the above equation gives $T_e=150$ eV. If $x=C_s\tau>L_R$, where C_s is the ion sound speed, a shock wave can be formed in the plasma. If the shock wave relaxation depth $\Delta x\sim(M/m)^{1/2}l_i$, where M, m are the ion and electron mass and l_i is the ion free path, is less than the wavelength of plasma wave λ_{pl}, the strong wave breaking of the wake field produced by the main pulse can occurr there; it can be a good source of injection. For temperature $T_e\sim150$ eV in a He gas jet, the ion sound speed is $C_s\sim5\times10^6$ cm/s and $x\sim100$ μm so that the effect appears for the laser pulse with $L_R\leqslant100$ μm. The shock wave can be generated in the jet with $\omega_{pl}l_i(M/m)^{1/2}/2\pi c\leqslant1$, which gives the density range of $N_i>5\times10^{18}$ cm^{-3}.

In the present paper, we study the effect of the laser prepulse on the injection and acceleration process experimentally and numerically via two-dimensional (2D) hydrodynamic and particle-in-cell (PIC) simulation. Spatial and energy distribution of accelerated electrons is measured depending on the nanosecond order prepulse contrast ratio and its shape for short (~50 μm) Rayleigh length.

II. EXPERIMENTAL SETUP

A. Supersonic gas jet

In this experiment, an intense and ultrashort laser pulse is focused on helium gas. In order to form a spatially localized gas column, i.e., to suppress the transverse expansion into vacuum due to the thermal and fluid motion of the injected gas, a supersonic pulsed gas injection is used as a target [17,18]. The pulsed gas jet is produced by a device that consists of an axially symmetric *Laval* nozzle [19] and a solenoid fast pulse valve [18]. The nozzle is designed to form $M_e=4.2$ flow for He ($\gamma=1.660$). Here M_e is the Mach number at the exit of the nozzle and γ is the ratio of specific heat. It has a 2.0 mm inner diameter at the exit. The typical experimental setup is shown in Fig. 1. The nozzle with the pulse valve is placed inside the vacuum chamber. The pulse valve is driven for 5 ms per shot at a repetition rate of 0.2 Hz. The stagnation pressure of the valve is varied from 5.0 to 20.0 atm. With these pressures, the density at the exit of the nozzle ranged from 7×10^{18} to 3×10^{19} cm^{-3}. The uniform density distributions with the sharp boundary of the gas jet column near the exit are experimentally characterized by interferometory. Using two turbo molecular pumps and an 850-l vacuum dump tank, the background pressure of the vacuum chamber is kept lower than 1.0×10^{-4} Torr during the gas jet operation.

B. Laser system

The 12 TW Ti:sapphire laser system (B.M. Industries, α-Line series) based on the chirped pulse amplification (CPA) technique generates up to 600 mJ, 50 fs laser pulses at a fundamental wavelength of 790 nm with a 10 Hz repetition rate. The laser power at the target in the vacuum chamber is up to 5 TW. As shown in Fig. 1, the *p*-polarized laser pulse with a diameter of 50 mm is delivered into the vacuum chamber through a vacuum laser transport line and is focused on the front edge of the helium gas jet column at a height of 1.3 mm from the nozzle exit with an $f/3.5$ off-axis parabolic mirror. Figure 2 gives a side view of the interaction region obtained by the CCD (charge coupled device) camera, and illustrates the gas jet and the focus point. Figure 3 shows a typical image of a laser focal spot at the target position that is imaged with a 20× objective lens onto a 14-bit CCD camera. The spatial resolution is 0.1 μm in the image with this system. To measure the spot size, the system is calibrated with a wire 10 μm in diameter set on the nozzle exit. The spot size is 7.5 μm in full width at $1/e^2$ of maximum. The maximum laser intensity on the target is estimated to be 1.0×10^{19} W/cm^2 so that the laser strength parameter a_0 exceeds 2.0. The measured Rayleigh length is approximately 53 μm for this spot. According to the specification of the laser system, the contrast ratio of the main pulse to prepulse preceding it by 8 ns is typically greater than 10^{-6} at the fundamental wavelength. In order to investigate the laser prepulse effect on the ejection of the electron from the gas jet, we control nanosecond-order laser prepulses by detuning

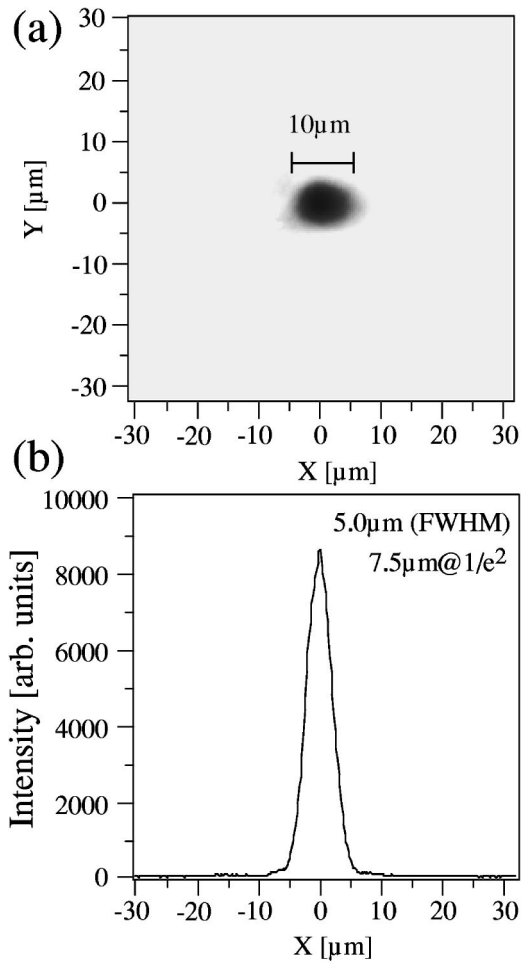

FIG. 3. (a) Image of the laser focal spot at the target. (b) Transverse profile of the spot.

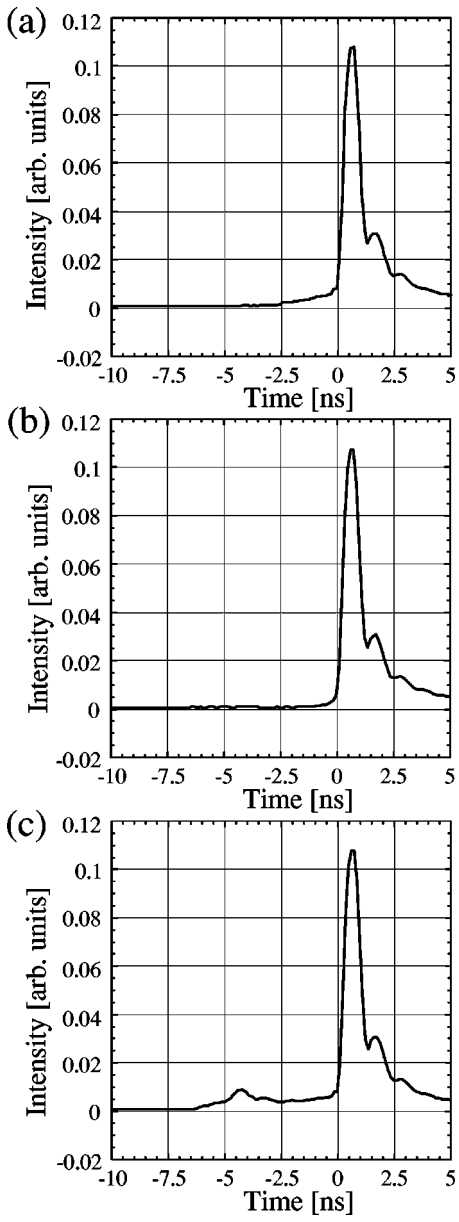

FIG. 4. Typical laser pulse shape detected by a photodiode. (a) ~2.5 ns prepulse, (b) ~1 ns prepulse, (c) ~5 ns nonmonotonic prepulse.

of a pockels cell of the regenerative amplifier of the laser system. The laser pulses are monitored by a photodiode behind a dielectric coated mirror set inside the vacuum laser transport line. Since the time resolution of the diode (~200 ps) is poor for the main pulse measurement but is enough to detect changes in nanosecond-order prepulse, the diode signals of the main pulse are calibrated with a third-order femtosecond cross correlator (Amplitude Technologies Sequoia). The typical laser pulses detected by the diode are shown in Figs. 4(a)–4(c). The prepulses usually range from −5 to −1 ns; here 0 corresponds to a beginning time of the main pulse. As shown in Fig. 4, the amplitude of the main pulse is kept constant for all prepulses by adjusting the pumping power of Nd:YAG (yttrium aluminum garnet) lasers for the multipass amplifier of the Ti:sapphire laser system.

C. Diagnostic setup

The spatial distribution of the electrons ejected from the gas jet is directly measured by a cup-shaped detector consisting of imaging plates (IP, Fuji film: BAS-SR) with a spatial resolution of 50 μm. The IP is a plastic film detector sensitive to high energy particles and radiation, which is used for electron microscopy and x-ray imaging. The cup has a wide accepted angle of 0°–50° from the forward laser axis for the ejected electrons. The imaging plates are laminated with an aluminum foil of 12 μm thickness on the surface to avoid exposure to x rays and the laser pulses. The bottom plate of the cup is placed 180 mm away from the focus point. The electron signals are accumulated over 300 shots. In order to obtain the energy distributions of the electrons, a magnetic electron deflector is set in the laser axis behind the jet (as shown in Fig. 1). The bottom plate of the cup (IP) is used as an electron detector. The deflector consists of a top and a bottom array of magnets that act as a permanent dipole magnet to disperse the electrons according to their kinetic energy. The magnetic field between the magnets is mapped out with a Hall probe and the maximum field strength reaches 300 mT. The deflector has an entrance aperture of 2.0 mm with

an acceptance solid angle of 1 msr. The trajectories of the electrons bent in the magnetic field and projected on the bottom plate of the cup are computed by a ray tracing. With this setup, the energy distribution of the ejected electrons up to 40 MeV can be detected. On the sidewall of the cup, the energy of electrons is estimated by a filtering with 100 μm polyethylene sheets stacked on the surface of the IP. The visible light emission from the plasma at the interaction region is observed in the direction of 90° from the laser propagation axis by a time-gated (20 ms) CCD camera (Hamamatsu C4880) with a spatial resolution of 12 μm. A blue-pass filter is put in front of the CCD camera to cut the laser light.

III. SIMULATION MODELS

To evaluate the effect of the laser prepulse, we numerically solve the hydrodynamics equation in the following form [16]:

$$\frac{\partial}{\partial t}n+\frac{\partial}{\partial \vec{r}}(n\vec{u})=0,$$

$$\frac{\partial}{\partial t}\vec{u}+\left(\vec{u}\frac{\partial}{\partial \vec{r}}\right)\vec{u}=-\frac{1}{Mn}\frac{\partial}{\partial \vec{r}}(znT)-\eta\Delta\vec{u},$$

$$\frac{\partial}{\partial t}(nT)+\frac{\partial}{\partial \vec{r}}\left(\frac{5}{3}\vec{u}nT\right)+n\frac{\partial}{\partial \vec{r}}\left(\kappa\frac{\partial}{\partial \vec{r}}T\right)$$

$$=\frac{8\pi e^2}{3mc\omega^2}\nu_{ei}nI_0\frac{d_0^2}{d_R^2}\exp(-0.5r^2/d_R^2), \qquad (1)$$

where n,z,M are the ion density, charge, and mass; T is the electron temperature, η,κ are the plasma viscosity and thermal conductivity, and $\nu_{ei}=4\pi e^2z^2n\Lambda/m^{1/2}T^{3/2}$ is the electron-ion collision frequency, where Λ is the Coulomb logarithm. The last term of the third equation describes laser energy deposition $d_R=d_0\sqrt{1+x^2/L_R^2}$, where d_0 is the laser spot size, x is the coordinate in the laser propagation direction, and L_R is the Rayleigh length.

The system of Euler equations (1) is solved numerically by a fully conservative scheme [20], assuming cylindrical symmetry, for a fully ionized He slab with 2.0 mm depth. The plasma density linearly increases from zero to maximal ion density $n=1.5\times10^{19}$ cm^{-3} after 300 μm, which is the focus point, and then the density is constant. The initial temperature is uniform and equals $T_0=0.1$ eV; the initial velocity is zero. Calculation is performed for the prepulse intensity $I_p=10^{13}$ W/cm^2 with duration 2.0 ns, $d_0=7.0$ μm, and $L_R=50$ μm. These parameters are chosen to be close to the experimental ones.

Longitudinal density distribution obtained from the hydrodynamics simulation is used for two-dimensional particle-in-cell simulation employing the moving window technique [9]. However, we neglect the effect of the transverse density distribution on the laser propagation, assuming that the cavity width is much larger than that of the laser spot size. The size of the window is 250 μm$\times$40 μm. The computational grid is 5000$\times$960. We use four particles per cell; there is no ionization included for this simulation. The initial laser field is chosen as a plane wave with E_Z and H_Y component with distribution as follows:

$$E_\gamma(x,y,t)=\frac{a_0}{f}\exp\{-i\omega t+ik[x+y^2/(2xf^2)]$$

$$-i\arctan(x/L_R)-y^2/(d_R)^2\}, \qquad (2)$$

where $a_0=eE_0/mc\omega$, x, y the longitudinal and transverse coordinates, $f=\sqrt{1+x^2/L_r^2}$; $k=c/\omega$. The maximal laser intensity is 2×10^{19} W/cm^2, $\lambda=0.79$ μm ($a_0=3.0$). The pulse duration [(FWHM) full width at half maximum] is 50 fs, as shown in Fig. 3 the focus spot size at $1/e^2$ of maximal intensity is 7.0 μm so that the Rayleigh length is estimated to be $L_R=50$ μm.

IV. RESULTS AND DISCUSSION

Figures 5(a)–5(c) (left-hand side) show the spatial distribution of electrons deposited on the bottom plate of the cup-shaped IPs. The distributions are obtained for different prepulse conditions [as shown in Figs. 4(a)–4(c)] and for gas density of 2.8×10^{19} cm^{-3} and 4.8 TW peak power of the main pulse. It is clearly seen that the spatial distribution of the ejection of electrons from the jet depends strongly on the laser prepulse. A peak distribution is observed at a density range of 7×10^{18} to 3×10^{19} cm^{-3}. In the first case, as shown in Fig. 5(a) (left-hand side), for a prepulse with a contrast ratio of $1:10^6$, pulse duration 2–3 ns, and energy $\sim$10% of the total pulse energy, corresponding to Fig. 4(a), a peaked spot distribution by narrow-cone ejection of electrons is clearly seen at the center of the plate. In the second case, as shown in Fig. 5(b) (left-hand side), for the prepulse with contrast ratio $1:10^6$ and pulse duration less than 1 ns with energy less than $\sim$10% of the total pulse energy, corresponding to Fig. 4(b), no electron signal is observed on the bottom plate. In the third case, as shown in Fig. 5(c) (left-hand side), for the prepulse with contrast ratio $1:10^6$, pulse duration more than 5 ns, and nonmonotonic pulse shape with energy more than $\sim$10% of the total pulse energy, corresponding to Fig. 4(c), the ejected electrons explode into pieces and smaller spots are detected at the bottom plate. This spotted distribution is measured even in a single shot. The radial and longitudinal distributions of the ion density in the He gas jet after the laser prepulse obtained by the hydrodynamic simulation are shown in Fig. 6. The radial distribution of the plasma (ion) density, shown in Fig. 6(a), is very close to those obtained experimentally in Refs. [11–15]. However, in the direction of laser pulse propagation, shown in Fig. 6(b), there is no preplasma channel that can give rise to an optical guiding. We should note that in a similar experiment (see Ref. [15]), performed with a longer Rayleigh length when optical guiding is crucial, the angular distribution of energetic electrons is very different from that measured in the present experiment. For the first case, after 2 ns of irradiation by the laser prepulse, there is a clearly seen

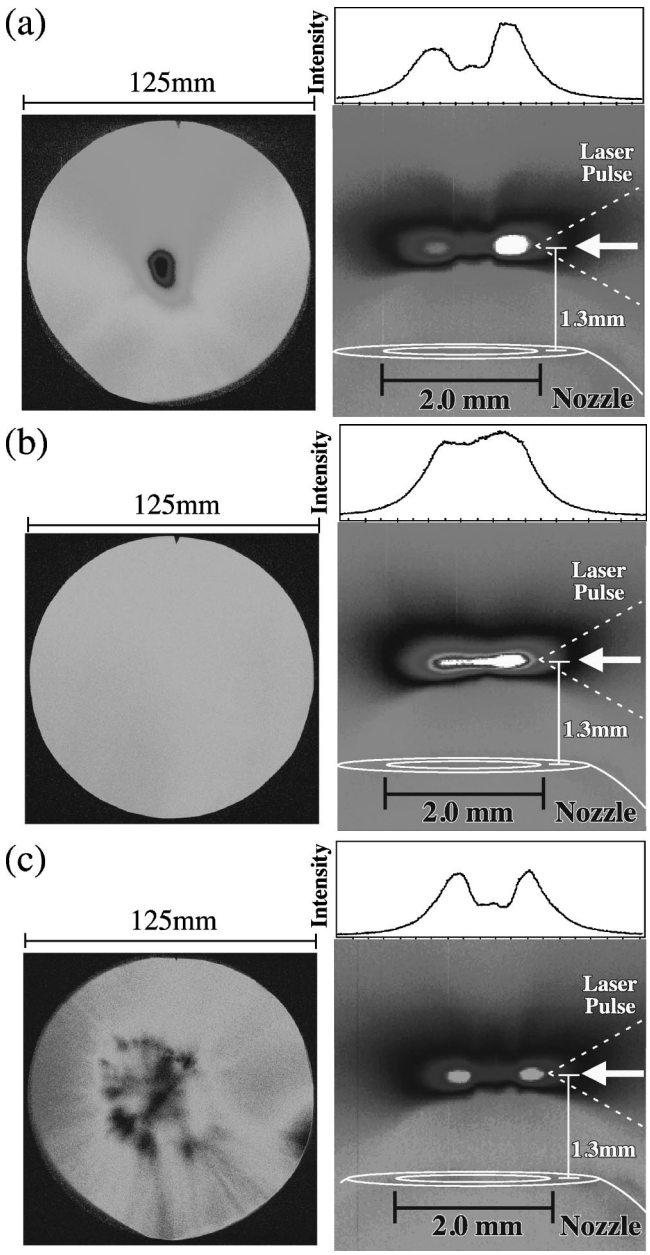

FIG. 5. Typical images of electrons deposited on the bottom plate of the cup-shaped IPs (left hand), and corresponding image of the plasma radiation (right-hand side), and longitudinal profile of the plasma radiation in the direction 90° from the axis (right up) obtained in a density of 2.8×10^{19} cm^{-3} and laser power of 4.8 TW. (a) ~2.5 ns prepulse, (b) ~1 ns prepulse, (c) ~5 ns nonmonotonic prepulse.

shock wave and the density gradient becomes steep at the front of the shock. The thickness of the shock wave, ~10 μm, is comparable to the plasma wavelength so that strong wave breaking and electron injection is expected for this condition. A condition of the pulse duration of 2–3 ns matches well with one of the shock wave formation also with consequent wave breaking of the wake field produced by the main laser pulse. For the prepulse intensity $I=10^{13}$ W/cm^2, the shock wave is formed after 1 ns of irradiation. This means if the laser prepulse is shortened two times, such as in

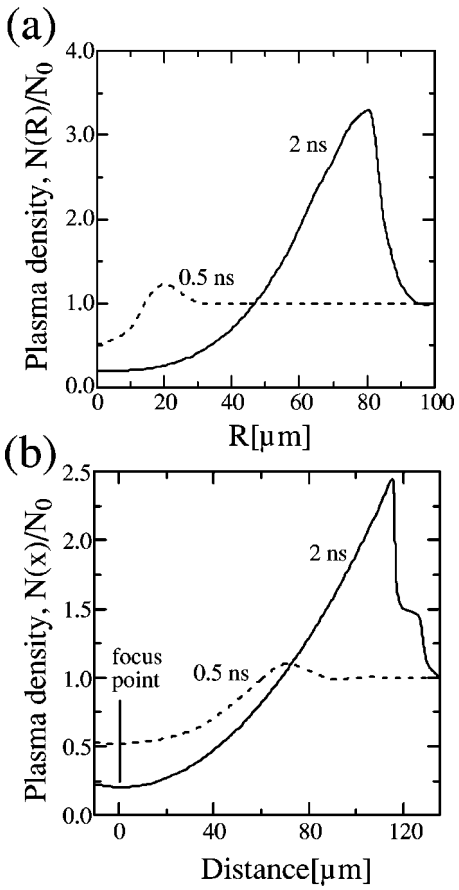

FIG. 6. Density distributions of a He jet after the laser prepulse calculated by 2D hydrodynamic simulation. The power density of the prepulse is 10^{13} W cm^{-2} and the Rayleigh length is 50 μm. (a) Radial direction ($x=0$), (b) longitudinal direction ($r=0$).

the second case, there should be no electron injection caused by the wave breaking into the consequent wake field. In addition, if the laser prepulse gets shorter and its energy decreases, the density distribution becomes uniform. This is because there is no shock wave in the cavity and the laser intensity is not strong enough to produce a wake field with an intensity higher than $E_B\sim[2(\omega/\omega_{pl}-1)]^{1/2}mc\omega_p/e$. The spotted distribution in the case of nonmonotonic laser prepulse is, we believe, a result of an instability at the shock wave. Since the condition for the wave breaking is dependent strongly on plasma dynamics, we expect that hydrodynamic disturbances in the shock front may strongly affect the process. Once it appears, the shock wave cannot decay rapidly. However, such a hydrodynamic instability disturbs the front of the shock wave. Since the injection of the main acceleration due to wave breaking must be directed along with the density gradient, this instability leads to the formation of spotted distribution. These results suggest that the laser prepulse affects the initial plasma density profile steepened in the direction of laser propagation due to the formation of a shock wave, which is essential for the injection into the consequent wake fields and the ejection of the narrow-cone electrons from the jet.

Figures 5(a)–5(c) (right-hand side) show the images of the radiation from the plasma obtained by the CCD camera

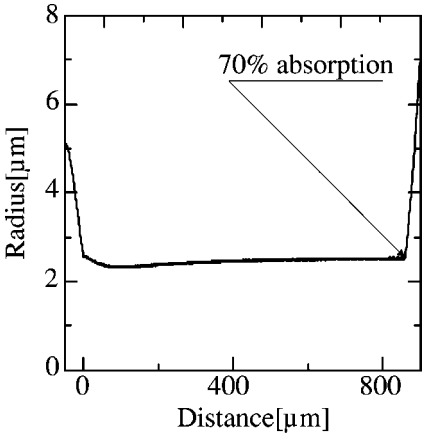

FIG. 7. The radius of the laser pulse (at 50% of the total pulse energy) with propagation distance.

in a direction 90° to the laser propagation axis, which corresponds to the spatial distributions of electrons shown on the left-hand side. The setup in the images corresponds to the one in Fig. 2. The longitudinal profile of the plasma radiation is also inset with the images. Figure 5(a) shows that the radiation from the plasma has a dumbbell shape; two bright spots at the edges and a narrow channel between them in the direction of the laser propagation. In this condition, the spot at the front edge is much brighter than that at the rear. Figure 5(b) shows that the plasma shape of the radiation for a smaller prepulse is uniform over the jet. In contrast to the case shown in Fig. 5(a), in the case of strong prepulse, shown in Fig. 5(c), the plasma also has the form of a dumbbell shape, though a brightness of the spots at the both edges are comparable. This proves that the visible radiation of the plasma depends on the prepulse as well. The radiation from the plasma is dominated by electrons because the rate of multiphoton excitation of He atoms is very small even for the laser intensity we use. Moreover, helium is fully ionized in the channel so that the radiation in the channel can be only recombination radiation. The result of 2D PIC calculation of the laser spot size during its propagation in the jet with the shock wave is shown in Fig. 7. Since the critical power for self-focusing [21] for the electron density $N_e=3\times10^{19}$ cm^{-3} is $P_c r=1.7\times10^{-2}n_c r/n$ TW$=0.9$ TW, the laser pulse with $P=4$ TW forms a laser channel. After passing distance $L\sim0.8$ mm, the pulse diffracts because its power becomes smaller than critical one. However, the laser energy absorbed by the electrons is only 58%, so that approximately 25% of the laser pulse energy is lost to diffraction during its propagation. Since the propagation length is smaller than the size of gas jet and the prepulse has small Rayleigh length, the plasma radiation at the rear of the channel is dominated by electrons propagating through the jet. If wave breaking occurs, the energy of the electrons passing through the jet becomes very high. Such electrons cannot efficiently ionize and the plasma spot at the rear becomes darker. We should note that a longer channel length ~0.8 mm correlates with the dark channel in radiation measurement.

The transverse profile of the spot of Fig. 5(a) (left-hand side) is shown in Fig. 8. The size of the spot is 8.1 mm

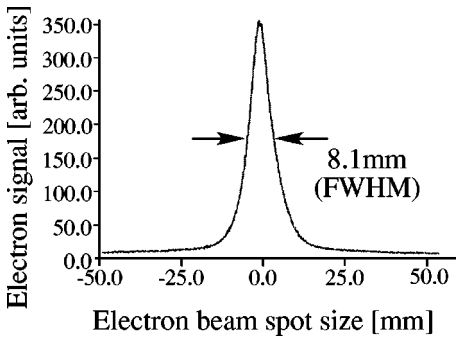

FIG. 8. Transverse profile of the peak spot electrons deposited on the bottom plate on cup-shaped IPs, which corresponds to Fig. 5(a).

(FWHM), which corresponds to a divergence angle of the ejection of $\sim2.5°$. The corresponding transverse geometrical emittance of the electron bunches is as small as $\sim0.1\pi$ mm mrad, though Coulomb explosion strongly affected the bunch in its propagation. However, the size of the spot for each shot may be smaller than that accumulated over 300 shots because of their pointing stability. The calculated charge of the single bunch is approximately 0.7 nC/ 1 J with a duration of 40 fs.

Electrons injected during wave breaking are further accelerated by the laser wake field. Figure 9 shows a typical energy distribution of the electrons ejected from the rear of the gas jet. The distribution is obtained by the spectrometer for a gas density of 1.4×10^{19} cm^{-3}, 4.0 TW peak power of the main pulse, and with a prepulse condition of the narrow-cone electron ejection as shown in Fig. 4(a). The aperture of the spectrometer allowed detection of only the narrow-cone electrons. A calculated electron energy distribution is also shown in Fig. 9. The electron spectrum has an exponential profile. Assuming that this distribution is a Maxwellian with an effective temperature T_h, we get $T_h\sim10$ MeV for both measured and calculated ones. They have a fairly good agreement for electron energy $E\leqslant40$ MeV. According to these

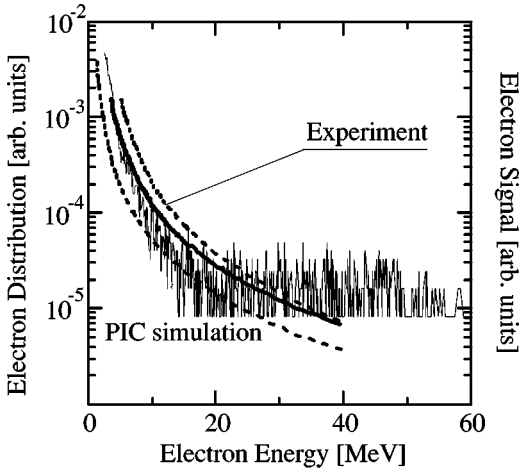

FIG. 9. The measured and calculated energy distribution of electrons in the bunch for a density of and 1.4×10^{19} cm^{-3} and a laser power of 4 TW. The dotted line shows experimental error.

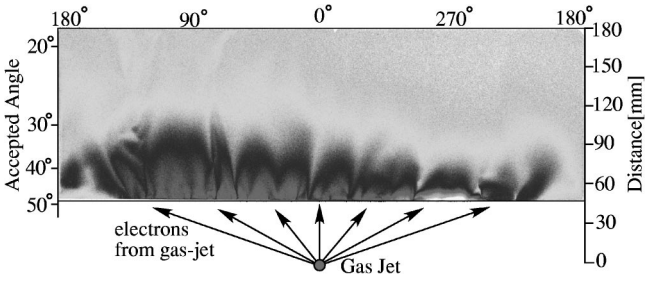

FIG. 10. Typical image of electrons deposited on a sidewall plate of the cup-shaped IPs, which corresponds to Fig. 5(a).

values, the acceleration gradient is evaluated to exceed 50 GV/m for the 800 μm acceleration distance. In the present paper, we do not measure the bunch duration; however, the PIC calculation gives 40 fs duration for an electron bunch composed of electrons with energy 10~40 MeV.

Figure 10 shows a typical spatial distributions of electrons deposited on the cylindrical wall of the cup-shaped IPs. The lower energy electrons (less than 500 keV) with a wide-cone ejection angle (larger than 30°) from the laser axis were observed. In contrast to the deposition on the bottom plate, significant changes to the distribution for the prepulse was not observed in any case. Since it was predicted that a transverse-wake wave breaking is insensitive to an initial density profile as compared to the longitudinal one [22], it may suggest injection due to the transverse-wake wave breaking. So it was found that there are two components of the ejection angle of the electrons with the narrow cone and the wide cone.

V. CONCLUSION

We have measured the spatial and energy distributions of electrons accelerated by an ultrashort laser pulse with short Rayleigh length. This acceleration depends strongly on the laser prepulse parameters.

In the condition where the prepulse forms a shock wave in the direction of laser propagation, the electron injection due to the plasma wave breaking occurs at the front of the shock. The narrow-cone electron bunch has been shown to appear due to the injection. For lower energy in the laser prepulse, less than ~10% of the energy of the main pulse, we have not observed the bunch, while for nonmonotonic prepulse, we believe, the hydrodynamic instability at the shock front dominates the spotted distribution of energetic electrons. A transverse geometrical emittance of 0.1π mm mrad has been observed. The energy distribution in the bunch is Maxwell-like with the effective temperature $T_h \sim 10$ MeV, and the maximal energy we observed is 40 MeV. The electrons with energy from 10 to 40 MeV constitute a bunch with a duration of 40 fs in PIC simulation. The calculated charge of the electron bunch is 0.7 nC/1 J.

ACKNOWLEDGMENTS

We are grateful to professor K. Horioka of the Tokyo Institute of Technology for his helpful discussions and encouragement. This research was partly supported by the advanced compact accelerator development office of the NIRS (National Institute of Radiological Sciences) and the REIMEI research resources of JAERI (Japan Atomic Energy Research Institute).

[1] T. Tajima and J. Dawson, Phys. Rev. Lett. **43**, 267 (1979).

[2] K. Nakajima, D. Fisher, T. Kawakubo, H. Nakanishi, A. Ogata, Y. Kato, Y. Kitagawa, R. Kodama, K. Mima, H. Shiraga, K. Suzuki, K. Yamakawa, T. Zhang, Y. Sakawa, T. Shoji, Y. Nishida, N. Yugami, M. Downer, and T. Tajima, Phys. Rev. Lett. **74**, 4428 (1995); F. Amiranoff, S. Baton, D. Bernard, B. Cros, D. Descamps, F. Dorchies, F. Jacquet, V. Malka, J.R. Marques, G. Matthieussent, P. Mine, A. Modena, P. Mora, J. Morillo, and Z. Najmudin, *ibid.* **81**, 995 (1998); F. Dorchies, F. Amiranoff, V. Malka, J.R. Marques, A. Modena, D. Bernard, F. Jacquet, Ph. Mine, B. Cros, G. Matthieussent, P. Mora, A. Solodov, J. Morillo, and Z. Najmudin, Phys. Plasmas **6**, 2903 (1999).

[3] D. Umstadter, S.-Y. Chen, A. Maksimchuk, G. Mourou, and R. Wagner, Science **273**, 472 (1996); D. Umstadter, J.K. Kim, and E. Dodd, Phys. Rev. Lett. **76**, 2073 (1996).

[4] E. Esarey, R.F. Hubbard, W.P. Leemans, A. Ting, and P. Sprangle, Phys. Rev. Lett. **79**, 2682 (1997).

[5] S.V. Bulanov, N. Naumova, F. Pegoraro, and J. Sakai, Phys. Rev. E **58**, R5257 (1998).

[6] M. Uesaka, K. Tauchi, T. Kozawa, T. Kobayashi, T. Ueda, and K. Miya, Phys. Rev. E **50**, 3068 (1994); M. Uesaka, T. Watanabe, T. Kobayashi, T. Ueda, K. Yoshii, G. Wu, X. Li, Y. Muroya, J. Sugahara, K. Kinoshita, N. Hafs, H. Okuda, T. Nishihara, Y. Terada, K. Nakajima, and Y. Katsumura, Radiat. Phys. Chem. **60**, 303 (2001); N. Hafz, M. Uesaka, J. Koga, and K. Nakajima, Nucl. Instrum. Methods Phys. Res. A **455**, 148 (2000).

[7] S.V. Bulanov, L.M. Kovrizhnykh, and A.S. Sakharov, Phys. Rep. **186**, 1 (1990); G.B. Whitham, *Linear and Nonlinear Waves* (Wiley, New York, 1974).

[8] S.V. Bulanov, V.I. Kirsanov, and A.S. Sakharov, JETP Lett. **53**, 565 (1991).

[9] R.G. Hemker, N.M. Hafz, and M. Uesaka, Phys. Rev. ST Accel. Beams **5**, 041301 (2002).

[10] J.D. Kmetec, C.L. Gordon III, J.J. Macklin, B.E. Lemoff, G.S. Brown, and S.E. Harris, Phys. Rev. Lett. **68**, 1527 (1992).

[11] J. Faure, V. Malka, J.-R. Marques, F. Amiranoff, C. Courtois, Z. Najmudin, K. Krushelnick, M. Salvati, A.E. Dangor, A. Solodov, P. Mora, J.-C. Adam, and A. Heron, Phys. Plasmas **7**, 3009 (2000).

[12] V. Malka, J. Faure, J.R. Marques, F. Amiranoff, P. Rousseau, S. Ranc, J.P. Chambaret, Z. Najmudin, B. Walton, P. Mora, and A. Solodov, Phys. Plasmas **8**, 2605 (2001).

[13] C.G. Durfee, J. Lynch, and H.M. Milchberg, Phys. Rev. E **51**, 2368 (1995).

[14] L.C. Johnson and T.K. Chu, Phys. Rev. Lett. **32**, 517 (1974).

[15] V. Malka, S. Fritzler, E. Lefebvre, M.-N. Aleonard, F. Burgy,

J.-P. Chambaret, J.-F. Chemin, K. Krushelnick, G. Malka, S.P.D. Mangles, Z. Najmudin, M. Pittman, J.-P. Rousseau, J.-N. Scheurer, B. Walton, and A.E. Dangor, Science **298**, 1596 (2002).

[16] Ya. B. Zelfdovich and Yu. P. Raizer, *Physics of Shock Waves and High-Temperature Hydrodynamics Phenomena* (Academic Press, New York, 1967), Vol. 1, p. 342; Vol. 2, p. 515.

[17] V. Malka, C. Couland, J.P. Geindre, V. Lopez, Z. Najmudin, D. Neely, and F. Amiranoff, Rev. Sci. Instrum. **71**, 2329 (2000); S. Semushin and V. Malka, *ibid.* **72**, 2961 (2001).

[18] T. Hosokai, K. Kinoshita, T. Watanabe, K. Yoshii, T. Ueda, A. Zhidkov, and M. Uesaka, in *Proceedings of EPAC 2002*, edited by T. Garvey, J. Le Duff, P. Le Roux, C. Petit Jean-Genaz, J. Poole, and L. Rivkin (EPS-IGA and CERN, Paris, 2002), p. 981.

[19] J.D. Anderson, Jr., *Modrrn Compressible Flow with Histrical Perspective*, 2nd ed. (McGraw-Hill, New York 1989), Chap. 5.

[20] A.A. Samarskii, E.S. Nikolaev, *Numerical Method for Grid Equations* (Birkhauser Verlag, Basel, 1989), Vol. 1 and 2.

[21] Guo-Zheng Sun, Edoward Ott, Y.C. Lee, and Parvez Guzdar, Phys. Fluids **30**, 526 (1987); A.B. Borisov, A.V. Borovskiy, O.B. Shiryaev, V.V. Korobkin, A.M. Prokhorov, J.C. Solem, T.S. Luk, K. Boyer, and C.K. Rhodes, Phys. Rev. A **45**, 5830 (1992).

[22] S.V. Bulanov, F. Pegoraro, A.M. Pukhov, and A.S. Sakharov, Phys. Rev. Lett. **78**, 4205 (1997).